

Point-contact spectroscopy in Co-doped CaFe_2As_2 : nodal superconductivity and topological Fermi surface transition.

R S Gonnelli¹, M Tortello¹, D Daghero¹, R K Kremer², Z Bukowski^{3,4}, N D Zhigadlo³, and J Karpinski³

¹ Dipartimento di Scienza Applicata e Tecnologia, Politecnico di Torino, corso Duca degli Abruzzi 24, 10129 Torino (TO) Italy

² Max-Planck-Institut für Festkörperforschung, D-70569 Stuttgart (Germany)

³ Laboratory for Solid State Physics, ETHZ, CH-8093 Zurich, Switzerland

⁴ Institute of Low Temperature and Structure Research, Polish Academy of Sciences, P.O. Box 1410, 50-422 Wrocław, Poland

E-mail: renato.gonnelli@polito.it

Abstract. We performed point-contact Andreev reflection spectroscopy measurements in $\text{Ca}(\text{Fe}_{1-x}\text{Co}_x)_2\text{As}_2$ single crystals with effective $x = 0.060 \pm 0.005$. The spectra of *ab*-plane contacts show a zero-bias maximum and broad shoulders at about 5-6 meV. Their fit with the three-dimensional Blonder-Tinkham-Klapwijk model (making use of an analytical expression for the Fermi surface that mimics the one calculated from first principles) shows that this compound presents a large isotropic gap on the quasi-2D electronlike Fermi surface sheets and a smaller anisotropic (possibly nodal) gap on the 3D holelike Fermi surface pockets centered at the Z point in the Brillouin zone. These results nicely fit into the theoretical picture for the appearance of nodal superconductivity in 122 compounds.

PACS numbers: 74.72.-h, 74.45.+c, 71.15.Mb

1. Introduction

Among the members of the 122 family of Fe-based superconductors, the CaFe_2As_2 system is particularly challenging from both the theoretical and the experimental points of view. With respect to Sr-122 and Ba-122, which have been widely studied in the past years and whose phase diagrams have been soon determined, the Ca-122 system presents some peculiarities (namely, a high sensitivity of the cell structure to chemical and physical pressure, and a strong dependence of the physical properties of single crystals on the growth procedure [1]) that have hindered its investigation and caused conflicts between data and calculations by different groups.

Recently, the phase diagram of $\text{Ca}(\text{Fe}_{1-x}\text{Co}_x)_2\text{As}_2$ as a function of x has been determined independently by Hu et al. [1] and Harnagea et al. [2]. Despite some small quantitative disagreement on the Co content, the two phase diagrams agree well with each other. In particular, unlike in the sister compounds $\text{Sr}(\text{Fe}_{1-x}\text{Co}_x)_2\text{As}_2$ and $\text{Ba}(\text{Fe}_{1-x}\text{Co}_x)_2\text{As}_2$, the superconducting phase appears abruptly (at $x = 0.03$ in Ref.[1]) where the high-temperature magnetic and structural transitions are still present, and the critical temperature gradually decreases with increasing x .

In this paper we present the results of point-contact Andreev-reflection spectroscopy (PCARS) measurements in $\text{Ca}(\text{Fe}_{1-x}\text{Co}_x)_2\text{As}_2$ single crystals with $x = 0.060 \pm 0.005$, aimed to determine the number, the amplitude and the symmetry of the superconducting order parameter(s) in this compound. These pieces of information, which were lacking up to now, are of particular interest if compared to the predictions about the dependence of the gap symmetry of 122 compounds on the shape of the Fermi surface (and thus on the height of the pnictogen above the Fe layer, h_{As}) [3]. We will show indeed that the PCARS results give evidence of a large isotropic gap and a small nodal (or fully anisotropic) gap, and that DFT calculations of the Fermi surface show a topological transition in the holelike Fermi surface sheets occurring at the same doping content. We speculate that the two facts may be correlated and that the symmetry of the OP on the closed holelike pockets at $x \geq 0.06$ can be modeled as a 3D d -wave one, with two nodal planes intersecting each other along the Γ -Z line.

2. Experimental results

The $\text{Ca}(\text{Fe}_{1-x}\text{Co}_x)_2\text{As}_2$ single crystals used in this work were grown from Sn flux, as described in Ref. [4]; they looked very similar to those shown in Ref. [2], i.e. they were plate-like, with mirror surfaces and the c axis perpendicular to the plate. The inset to Fig.1 shows the DC magnetization of one of the crystals as a function of temperature. The transition sets in at $T_c^{\text{on}} = 20$ K and an effective $T_c^{\text{eff}} = 17$ K can be determined by extrapolating the linear part of the curve. The rather broad transition is common to all the state-of-the-art single crystals grown at present [1, 2, 5, 6]. The broadening might be related to chemical inhomogeneities over nanoscopic length scales [2] that are not detectable by energy- or wavelength-dispersive X-ray spectroscopies [2, 1], or might be

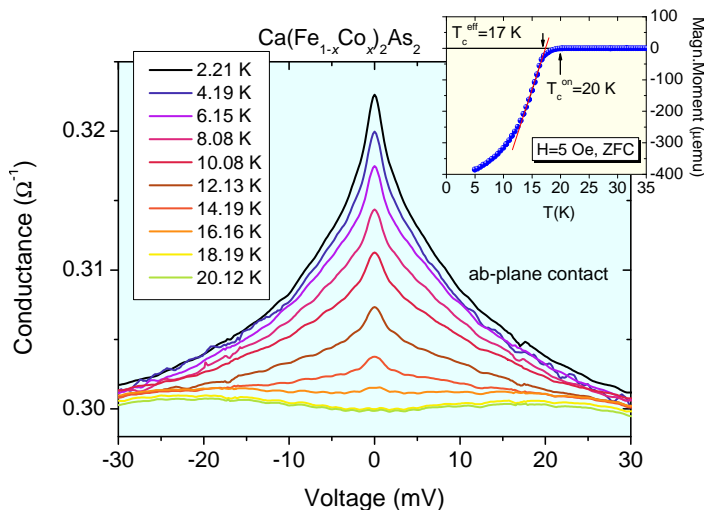


Figure 1. Some experimental conductance curves (not normalized) as a function of temperature. The point-contact resistance is about 3Ω . Inset: the zero-field-cooled DC magnetization of one of our crystals.

intrinsic to the Ca-122 system because of its high sensitivity to chemical and physical pressure [2]. In any case, the large transition width is not detrimental to point-contact measurements since PCARS is a local probe not only of the superconducting order parameter but also of the critical temperature. The critical temperature of the best contacts always fell between T_c^{eff} and T_c^{on} . By comparison with the phase diagram by Hu *et al.* [1], we can conclude that the real Co content of our crystals is $x = 0.060 \pm 0.005$.

The point-contact measurements were performed by using the “soft” technique described elsewhere, i.e. by putting a small drop of Ag paste ($\phi \simeq 50 \mu\text{m}$) on a fresh side surface of the crystal (exposed by breaking it) so that the current is mainly injected along the *ab* planes. Contacts made in this way are more mechanically and thermally stable than those made by using the standard needle-anvil technique (i.e. by gently pressing a sharp metallic tip against the same surface). The $I - V$ characteristics of the normal metal/superconductor junctions obtained in this way were measured and numerically differentiated to obtain the conductance curves, dI/dV vs. V .

Figure 1 shows the temperature dependence, from 2.21 K up to 20.12 K, of the raw conductance curves of a *ab*-plane point contact whose normal-state resistance was $R_N \simeq 3 \Omega$. The Andreev signal disappears completely at $T_c^A \simeq 18 \text{ K}$, leaving a slightly bent but rather symmetric normal-state conductance. Despite the rather low resistance, the conduction through the contact is very likely to be ballistic. This is witnessed by the fact that the high-energy tails of the curves coincide with one another (which means that there is no contribution from the Maxwell term in the contact resistance [7]), by the absence of features associated with the current-induced suppression of superconductivity (such as characteristic dips [8]) and by the fact that the Andreev critical temperature T_c^A is not suppressed with respect to the bulk T_c . The small resistance of the contact

can indeed be reconciled with the evidence of ballistic conduction if multiple parallel nanocontacts are formed between Ag grains in the paste and the crystal surface, which is not only very reasonable but practically unavoidable in our point contacts.

Even at a first glance, the shape of the curves in Fig.1 looks not to be compatible with a nodeless gap (or multiple nodeless gaps, as observed in most 1111 compounds [9] and in 122 compounds like $\text{Ba}(\text{Fe},\text{Co})_2\text{As}_2$ [10] and $(\text{Ba},\text{K})\text{Fe}_2\text{As}_2$ [11]). It must be noted that this shape is common to all the conductance spectra in the Andreev-reflection regime we obtained in different *ab*-plane contacts, so that it appears to be an intrinsic feature of the material and not an artifact. A narrow maximum at zero bias such as that shown in the curves in Fig.1 has been observed in many unconventional superconductors, including iron pnictides [12, 13, 14]; however, this kind of feature can have either intrinsic or extrinsic origins. For example, it can be the hallmark of a Josephson supercurrent – but this requires either the formation of some SIS junction, or intrinsic Josephson effects as in *c*-axis tunnelling in layered materials, both excluded here. Alternatively, the zero-bias peak can also be due to the non-perfectly ballistic conduction (already excluded for our contacts), or the local damage or deformation of the surface due to the pressure applied by the tip (see [7] and references therein), but this is clearly impossible with our technique. Finally – and we claim this is the case in our measurements – it can be a direct consequence of the anisotropy of the superconducting order parameter.

If the OP has nodal lines crossing the Fermi surface, as in the *d*-wave or in the nodal *s* symmetries proposed for 1111 pnictides in suitable conditions [15], its change of sign can give rise – for suitable directions of current injection – to constructive interference between hole-like and electron-like quasiparticles that result in zero-energy bound states localized at the interface [16]. These, in turn, manifest themselves in a zero-bias peak in the Andreev-reflection conductance. In principle, also the 3D nodal symmetry of the OP proposed for the isovalent-doped Ba-122 system [3, 17] could give rise to these effects. A similar peak can also appear in diffusive metal/nodal superconductor junctions as a result of the coherent Andreev reflection in the former [18].

We have however recently shown [9] that, in the presence of a large spectral broadening (as in our contacts on $\text{Ca}(\text{Fe}, \text{Co})_2\text{As}_2$) it becomes impossible to distinguish a true zero-bias conductance peak (due to a nodal OP) from the zero-bias maximum that is the natural consequence of a OP with zeroes on the Fermi surface. Strictly speaking, we can thus conclude that the shape of the conductance curves of Fig.1 indicates that at least some component of the OP is zero somewhere on the Fermi surface – although we cannot say whether it changes sign or not.

To extract quantitative information on the number, amplitude and symmetry of the OPs (with the aforementioned limitations), it is necessary first to normalize the experimental conductance curves and then to compare them with the predictions of suitable models for Andreev reflection. The first step is straightforward in this case, since the normal-state conductance is well defined and, judging from the superposition of the high-energy tails of the curves, seems not to depend very much on temperature

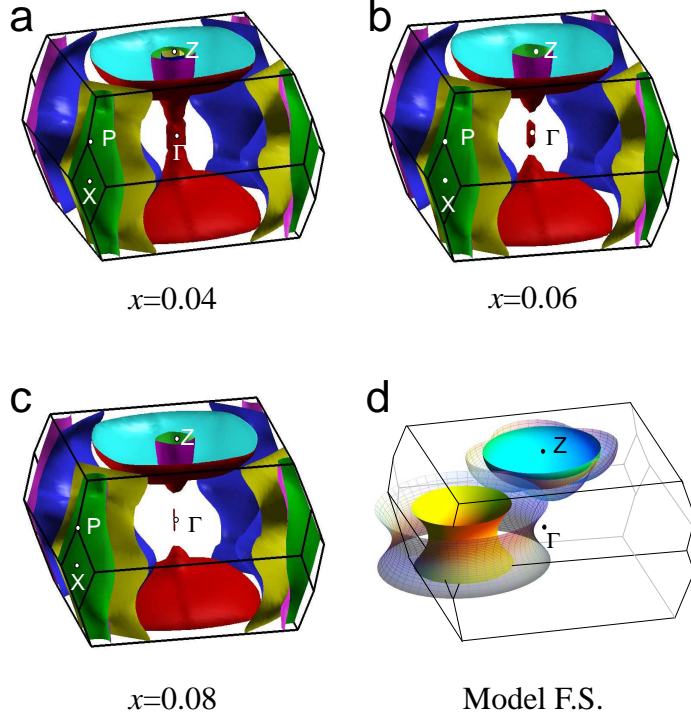


Figure 2. (a) The Fermi surface of $\text{Ca}(\text{Fe}_{0.96}\text{Co}_{0.04})_2\text{As}_2$ calculated as described in the text (Elk FP-LAPW code, GGA + VCA approach) by using the low-temperature lattice parameters of the collapsed tetragonal structure of CaFe_2As_2 from Ref.[19]. (b, c) the same as in (a) but for $x = 0.060$ and $x = 0.080$, respectively. (d) Model Fermi surface used to perform the 3D-BTK fit of the experimental PCAR curves (matt surfaces) and the relevant amplitude of the order parameter (gridded surfaces). Only one half of the two Fermi surfaces is shown.

below T_c^A . Therefore, we will divide every conductance curve at $T < T_c^A$ by a curve measured just above T_c^A . In the case of Fig.1, we used the curve at 18.19 K. As for the fit of the normalized conductance curves, one might choose for simplicity a two-band 2D-BTK model [16]. This model is actually based on the assumption that the Fermi surface is approximately cylindrical, but in 122 compounds a more or less pronounced warping of the Fermi cylinders is present already in the parent compounds, and increases with doping [17]. In the next section we will show that the 2D approximation for the Fermi surface is not justified in $\text{Ca}(\text{Fe}_{0.94}\text{Co}_{0.06})_2\text{As}_2$ so that the more complicated two-band 3D-BTK model must be used instead.

3. Calculation of the Fermi surface

To gain further insight into the real band structure of $\text{Ca}(\text{Fe}_{1-x}\text{Co}_x)_2\text{As}_2$ we performed first-principle DFT calculations by using the Elk FP-LAPW Code (<http://elk.sourceforge.net/>) within the GGA approach for the exchange correlation potential. A virtual-crystal approximation (VCA) was used to mimic the Co doping,

owing to the fact that VCA works particularly well for Fe-Co substitutions. In the absence of direct experimental information on the low-temperature lattice constants of Co-doped CaFe_2As_2 , we used the values $a = b = 3.925 \text{ \AA}$ and $c = 11.356 \text{ \AA}$, calculated in Ref. [19] *at low temperature* for the collapsed tetragonal phase of CaFe_2As_2 and obtained from the total energy minimization by considering the stripe antiferromagnetic order. Owing to the small doping dependence of the lattice constant at high temperature [1], we assumed these values to be a good first approximation to the real ones at the doping content of our interest ($x < 0.08$). The values of the theoretical parameters are in good agreement with the experimental ones measured in the collapsed tetragonal phase of the parent compound at 40 K (and pressure $P = 0.5 \text{ GPa}$ [20]). Starting from the calculated equilibrium phase and always considering the antiferromagnetic phase, an optimized internal parameter $z_{\text{As}} = 0.7306$ (such that $h_{\text{As}} = 1.309 \text{ \AA}$) was obtained. The charge density was thus integrated over $8 \times 8 \times 4$ k points in the Brillouin zone and the band structures as well as the Fermi surfaces were calculated in the non-magnetic body-centered tetragonal phase.

Figures 2(a), (b) and (c) show the Fermi surface (plotted on a $40 \times 40 \times 40$ k -points grid) of $\text{Ca}(\text{Fe}_{1-x}\text{Co}_x)_2\text{As}_2$ for $x = 0.04$, $x = 0.06$ and $x = 0.08$, respectively. The evolution of the holelike Fermi surface towards a full 3D nature on increasing x is clear. In the $x = 0.04$ case (panel a), three holelike FS sheets are present: two inner closed pockets centered at Z and an outer, strongly warped cylinder extending along the Γ -Z line. At $x = 0.06$ the smaller pocket disappears and the warped cylinder undergoes a topological transition splitting into separated closed surfaces centered at Z. It is worth noting that this trend is qualitatively robust against the details of the calculations, although some refinement (e.g. the relaxation of the cell parameters or their small doping dependence) could slightly change the doping content at which the complete separation of the two closed sheets around Z occurs.

4. Analysis of the experimental data

In these conditions, it is necessary to use the complete 3D-BTK model [9] to fit our conductance curves. We first schematized the actual Fermi surface of $\text{Ca}(\text{Fe}_{0.94}\text{Co}_{0.06})_2\text{As}_2$ by means of a one-sheeted hyperboloid of revolution (that simulates the electronlike FS sheets centered in X) and an oblate spheroid (to simulate the 3D holelike FS centered in Z). Fig.2(d) shows one half of the two model Fermi surfaces (corresponding to the upper half of the real Brillouin zone shown in panel (b)). The proportions between the size of the two FSs have been respected, though the distance between them (which is irrelevant in the following calculation) has been increased for clarity with respect to the actual distance shown in fig.2b. For this reason the Brillouin zone sketched in Fig.2d appears wider than the actual one and should be just considered as a guide to the eye.

Before proceeding, we had to make a guess about the symmetry of the two OPs residing on the two FSs. According to recent theoretical predictions, in the Ba-122

system an evolution from a pure $s\pm$ gap symmetry towards a peculiar 3D nodal one is expected when the pnictogen height z_{As} is reduced, for example by isovalent P doping [3]. It is interesting to note that the reduction in z_{As} simply leads to a larger holelike Fermi surface around the Z point, similar to the one depicted in Fig. 2(a). In these conditions, a three-dimensional sign change of the OP takes place within this Fermi surface near the edge of the Brillouin zone [3, 17], while the gap on the electron Fermi surface always remains fully open. When the holelike FS is further deformed into separated closed surfaces, as in our case, the symmetry of the OP relevant to it must evolve as well. We guess that the result of this evolution can be expressed as a 3D d -wave OP, whose expression in the reciprocal space is $\Delta(\theta, \phi) = \Delta \cos(2\theta) \sin^2(\phi)$, θ being the azimuthal angle in the (k_x, k_y) plane of the reciprocal space and ϕ the inclination angle. This OP features two orthogonal nodal planes intersecting along the Γ -Z line. As for the electronlike FS sheets, we assume that the relevant OP keeps a s -wave symmetry. The amplitude of the two OPs are shown in Fig.2(d) as gridded surfaces.

Now the theoretical conductance curve can be calculated, within some reasonable assumptions, by means of equation 9 of Ref.[9]. The two bands will be indicated by the subscripts 1 (holelike band) and 2 (electronlike band). The degrees of freedom of the problem are 7: the OP amplitudes Δ_1 and Δ_2 , the barrier parameters Z_1 and Z_2 , the broadening parameters Γ_1 and Γ_2 , plus the angle α between the direction of current injection (here in the basal plane) and the lobes of the d -wave gap Δ_1 . The relative weight of the two bands in the conductance is not an adjustable parameter but directly follows from the geometry of the problem (i.e. the shape of the relevant Fermi surface sheets and the direction of current injection) and from the choice of the Z parameters.

Figure 3(a) shows some of the experimental conductance curves of Fig.1, normalized and compared to the best-fitting curves (lines) calculated within the aforementioned model. The parameters that allow fitting the low-temperature curve are the following: $\Delta_1 = 1.7$ meV, $\Delta_2 = 5.3$ meV, $Z_1 = 0.4$, $Z_2 = 0.185$, $\Gamma_1 = 1.66$ meV and $\Gamma_2 = 6.4$ meV. The high values of the Γ parameters are due to the smallness of the Andreev signal. Such large values could be avoided by introducing an additional scaling parameter S sometimes used in these cases [21], for instance to account for a fraction of injected current that does not give rise to Andreev reflection. To reproduce the ZBCP a misorientation angle $\alpha = \pi/8$ was necessary. This value is quite reasonable because the side surfaces of the crystals, on which the point contacts are made, are rather irregular and thus the angle of current injection in the basal plane is not well defined. Indeed, it can be shown that the conductance curve one would obtain by averaging over all angles α between 0 and $\pi/4$ is best described by using a single $\alpha \simeq \pi/8$. Note that the values of the gaps given by this fit are very similar to those obtained by using a simplified 2D BTK model as in Ref.[9], but the Z values are systematically smaller because of the Z -enhancing effect discussed elsewhere [9]. Moreover, as already explained, similar results could be obtained by fitting the experimental normalized curves with a s -wave OP on one band and a *fully anisotropic s*-wave OP (with zeros on the Fermi surface) on the other band. It is also worth noting that a simpler model with a smaller number

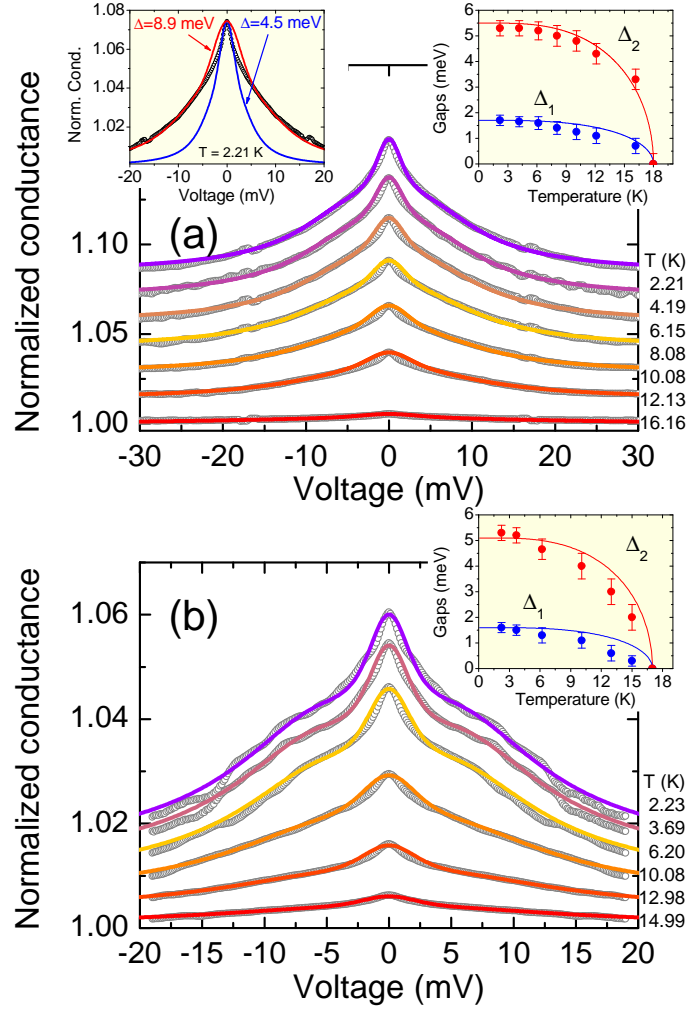


Figure 3. (a) Normalized conductance curves of the same contact as in Fig. 1 (symbols) and their relevant 3D-BTK fit obtained by using the model Fermi surface of Fig.2d (lines). The left inset shows two different one-gap, d -wave BTK fits (lines) to the low-temperature curve of the main panel (symbols). The values of the fitting parameters are: $\Delta = 8.9$ meV, $\Gamma = 6.2$ meV, $Z = 1.1$, $\alpha = \pi/8$ for the red, wider curve, and $\Delta = 4.5$ meV, $\Gamma = 3.2$ meV, $Z = 1.1$, $\alpha = \pi/8$ for the blue narrow curve. (b) Same as in (a) but for a different contact, with normal-state resistance $R_N \simeq 3.4\Omega$. Both in (a) and (b) the right insets report the values of the gap amplitudes Δ_1 and Δ_2 (circles) as a function of temperature. Lines represent two BCS-like temperature dependencies of the usual approximated form $\Delta_i(T) = \Delta_i(0) \tanh(1.74\sqrt{(T_c/T) - 1})$.

of parameters fails to reproduce the experimental conductance curves. The left inset to Fig.3(a) shows that a single-gap d -wave model (with 4 parameters) can only reproduce either the zero bias maximum (blue line) or the higher energy portion of the conductance curve (red line). Though the latter curve is better, the one-band fit is still less accurate than the two-band one; moreover, it would give an unreasonably large value of the gap.

Fig.3(b) shows the temperature dependence of the normalized conductance curves (symbols) of a different point contact, whose normal-state resistance was $R_N \simeq 3.4\Omega$.

As in panel (a), the experimental data are compared to the 3D-BTK best-fitting curves calculated for a large isotropic gap and a smaller d -wave gap. The fitting parameters at the lowest temperature are $\Delta_1 = 1.6$ meV, $\Delta_2 = 5.3$ meV, $Z_1 = 0.35$, $Z_2 = 0.265$, $\Gamma_1 = 2.2$ meV, $\Gamma_2 = 6.8$ meV and finally $\alpha = \pi/7.5$. The values of the broadening parameters are even higher than in the previous case, because the signal is smaller, but the values of the gaps are in very good agreement with those obtained from the curves in Fig.3(a). Some small additional structures are also visible in the lowest-temperature curves at about 8 and 12 meV that are not reproduced by the fit. These features might be related to a strong electron-boson interaction, as shown in Refs. [9, 10]. However, in this case we did not observe them in a reproducible way, and moreover they disappear soon with increasing temperature and the Andreev signal is too small to draw any conclusion in this sense. It is worth mentioning that such features contribute very little to the uncertainty of the gap values, which mostly arises from the smallness of the Andreev signal, as discussed below.

As shown in Fig.3(a) and (b), we were able to fit the conductance curves at any temperature up to T_c^A by using the same model and keeping the barrier parameters (Z_1 and Z_2) and the angle α independent of temperature. The amplitudes of the gaps, Δ_1 and Δ_2 , are shown as a function of temperature in the right insets to Fig.3(a) and (b). Error bars indicate the spread of gap values obtained in different fits of the same curve, with different combinations of the remaining parameters (Z_i , Γ_i and α). Because of the smallness of the Andreev signal, this spread at low temperature is of the order of 0.2 meV on Δ_1 and 0.3 meV on Δ_2 , and increases on heating. For the sake of comparison, the same insets also show two BCS-like trends – approximately expressed as $\Delta_i(T) = \Delta_i(0) \tanh(1.74\sqrt{(T_c^A/T) - 1})$, where $\Delta_i(0)$ is the low-temperature gap and T_c^A the experimental critical temperature of the contact. While the data of panel (a) look fairly compatible with these trends, some suppression of the gaps are observed in the inset to panel (b) in the proximity of T_c^A . The gap ratios turn out to be $2\Delta_1/k_B T_c^A = 2.2 - 2.3$ (much smaller than the BCS value for d -wave superconductors) and $2\Delta_2/k_B T_c^A = 6.85 - 7.25$, which is instead suggestive of a strong electron-boson coupling.

5. Conclusions

We have presented the results of point-contact Andreev reflection measurements in state-of-the-art $\text{Ca}(\text{Fe}_{1-x}\text{Co}_x)_2\text{As}_2$ single crystals with effective $x = 0.060 \pm 0.005$. The point contacts were made on the side surface, i.e. the current was mainly injected along the ab planes. We have shown that the shape of the PCARS spectra can be nicely explained within a multiband (multigap) scenario where a large isotropic gap Δ_2 coexists with a smaller nodal (or fully anisotropic) gap Δ_1 . These two gaps can be associated to the electronlike and holelike Fermi surface sheets, respectively, on the basis of recent theoretical papers [17, 3] that predict the development of 3D nodes in the OP of the holelike FS when the size of the latter around the Z points of the Brillouin zone

increases (for example, in Ba-122, as a consequence of P doping). We have shown by first-principle DFT calculations that Co doping in CaFe_2As_2 has a similar, but even more pronounced, effect on the holelike FS, which actually undergoes a topological transition at about $x \simeq 0.06$ from a warped cylinder along the Γ -Z line to separate ellipsoids centered around the Z points. In these conditions, we have assumed that the symmetry of the nodal gap Δ_1 can be described by a 3D d -wave function, while Δ_2 keeps a s -wave symmetry. The fit of the experimental spectra with a two-band 3D-BTK model using a model Fermi surface that simulates the calculated one gives $\Delta_2 = 5.3 \pm 0.3$ meV and $\Delta_1 = 1.6 \pm 0.2$ meV.

In conclusion, our results seem to confirm and extend the existing predictions about the evolution of the gap symmetry as a function of isovalent doping, and might suggest a connection between the topological transition of the holelike FS and the appearance of nodal points in the gap along the Γ -Z line. Further point-contact measurements in other Fe-based compounds and with the current injected in different directions could further substantiate this picture.

Acknowledgments

The work at Politecnico di Torino was supported by the PRIN Project No. 2008XWLWF9-005. The work at ETHZ was supported by the NCCR Project MaNEP. The authors thank very much G. Profeta for suggestions and enlightening discussions. R.S.G. acknowledges R. K. Kremer and the Max Planck Institute for Solid State Research in Stuttgart where the measurements were carried out.

References

- [1] Hu R, Ran S, Bud'ko S, Straszheim W E and Canfield P C 2011 Single crystal growth and superconductivity of $\text{Ca}(\text{Fe}_{1-x}\text{Co}_x)_2\text{As}_2$ unpublished, arXiv:1111.7034
- [2] Harnagea L, Singh S, Friemel G, Leps N, Bombor D, Abdel-Hafez M, Wolter A U B, Hess C, Klingeler R, Behr G, Wurmehl S and Buchner B 2011 *Phys. Rev. B* **83** 094523
- [3] Suzuki K, Usui H and Kuroki K 2011 *J. Phys. Soc. Jpn.* **80** 013710
- [4] Matusiak M, Bukowski Z and Karpinski J 2010 *Phys. Rev. B* **81** 020510(R)
- [5] Abdel-Hafez M, Harnagea L, Singh S, Stockert U, Wurmehl S, Klingeler R, Wolter A U B and Buchner B 2011 Calorimetric study of the superconducting and normal state properties of $\text{Ca}(\text{Fe}_{1-x}\text{Co}_x)_2\text{As}_2$ unpublished, arXiv:1109.3135
- [6] Kumar N, Nagalakshmi R, Kulkarni R, Paulose P L, Nigam A K, Dhar S K and Thamizhavel A 2009 *Phys. Rev. B* **79** 012504
- [7] Daghero D and Gonnelli R 2010 *Supercond. Sci. Technol.* **23** 043001
- [8] Sheet G, Mukhopadhyay S and Raychaudhuri P 2004 *Phys. Rev. B* **69** 134507
- [9] Daghero D, Tortello M, Ummarino G and Gonnelli R S 2011 *Rep. Prog. Phys.* **74** 124509
- [10] Tortello M, Daghero D, Ummarino G A, Stepanov V A, Jiang J, Weiss J D, Hellstrom E E and Gonnelli R S 2010 *Phys. Rev. Lett.* **105** 237002

- [11] Szabó P, Pribulová Z, Pristáš G, Bud'ko S L, Canfield P C and Samuely P 2009 *Phys. Rev. B* **79** 012503
- [12] Lu X, Park W K, Yuan H Q, Chen G F, Luo G L, Wang N L, Sefat A S, McGuire M A, Jin R, Sales B C, Mandrus D, Gillett J, Sebastian S E and Greene L H 2010 *Supercond. Sci. Technol.* **23** 054009
- [13] Yates K A, Cohen L F, Ren Z A, Yang J, Lu W, Dong X L and Zhao Z X 2008 *Supercond. Sci. Technol.* **21** 092003
- [14] Samuely P, Szabó P, Pribulová Z, Tillman M, Bud'ko S L and Canfield P C 2009 *Supercond. Sci. Technol.* **22** 014003
- [15] Kuroki K, Usui H, Onari S, Arita R and Aoki H 2009 *Phys. Rev. B* **79** 224511
- [16] Kashiwaya S and Tanaka Y 2000 *Rep. Prog. Phys.* **63** 16411724
- [17] Graser S, Kemper A F, Maier T A, Cheng H P, Hirschfeld P J and Scalapino D J 2010 *Phys. Rev. B* **81** 21450
- [18] Tanaka Y, Nazarov Y V, Golubov A A and Kashiwaya S 2004 *Phys. Rev. B* **69** 144519
- [19] Colonna N, Profeta G, Continenza A and Massidda S 2011 *Phys. Rev. B* **83** 094529
- [20] Mittal R, Mishra S K, Chaplot S L, Ovsyannikov S V, Greenberg E, Trots D M, Dubrovinsky L, Su Y, Brueckel T, Matsuishi S, Hosono H and Garbarino G 2011 *Phys. Rev. B* **83** 054503
- [21] Naidyuk Y G, Kvitnitskaya O E, Tiutrina L V, Yanson I K, Behr G, Fuchs G, Drechsler S L, Nenkov K and Schultz L 2011 *Phys. Rev. B* **84** 094516